Check for updates

Remotely Light-Powered Soft Fluidic Actuators Based on Plasmonic-Driven Phase Transitions in Elastic Constraint

Fabian Meder,* Giovanna Adele Naselli, Ali Sadeghi,* and Barbara Mazzolai*

Materials capable of actuation through remote stimuli are crucial for untethering soft robotic systems from hardware for powering and control. Fluidic actuation is one of the most applied and versatile actuation strategies in soft robotics. Here, the first macroscale soft fluidic actuator is derived that operates remotely powered and controlled by light through a plasmonically induced phase transition in an elastomeric constraint. A multiphase assembly of a liquid layer of concentrated gold nanoparticles in a silicone or styrene–ethylene–butylene–styrene elastic pocket forms the actuator. Upon laser excitation, the nanoparticles convert light of specific wavelength into heat and initiate a liquid-to-gas phase transition. The related pressure increase inflates the elastomers in response to laser wavelength, intensity, direction, and on–off pulses. During laser-off periods, heating halts and condensation of the gas phase renders the actuation reversible. The versatile multiphase materials actuate—like soft "steam engines"—a variety of soft robotic structures (soft valve, pnue-net structure, crawling robot, pump) and are capable of operating in different environments (air, water, biological tissue) in a single configuration. Tailored toward the near-infrared window of biological tissue, the structures actuate also through animal tissue for potential medical soft robotic applications.

Strategies for actuating flexible materials are a key resource for soft robotics,[1–3] providing that the mechanisms integrate without disturbing the benefits of the soft structure by undesired rigidity. Consequently, novel soft actuation strategies are sought, with boosted functionality in the elastic regime and capable of being fabricated and combined with soft structures.[1] One of the most versatile strategies of actuating soft robots is fluidic actuation.[4–6] Tailoring the structural anisotropy of the flexible actuators pressurized by gasses or liquids enables expansion, bending, twisting, and contracting motion while reducing overall complexity to a minimum—an elastic structure and a pressure source.[6] This actuation strategy is realized in nature and the plant kingdom by varying turgor pressures and water flux[7,8] In soft robotics, the pressure variation causing expansion of an elastic structure is obtained by

F. Meder, G. A. Naselli, A. Sadeghi, B. Mazzolai
Istituto Italiano di Tecnologia
Center for Micro-BioRobotics
Viale Rinaldo Piaggio 34, Pontedera, 56025 Pisa, Italy
E-mail: fabian.meder@iit.it; alisaadeghi@gmail.com;
barbara.mazzolai@iit.it

The ORCID identification number(s) for the author(s) of this article can be found under https://doi.org/10.1002/adma.201905671.

pumps, pressurized gas containers, combustion, chemical reactions, and phase transitions.[6,9–11] Often rigid and bulky components of classic fluidic circuits (such as bulky valves, tubes, and pumps tethered to the devices) are necessary and untethering is still a big challenge in soft robotics with fluidic actuation.[2,9,12–15]

New materials with embodied functionality capable of actuation provide essential potential for further developing soft robotic systems such as light-driven systems that enabling not only untethering but also drastically reducing complexity by providing integrated functionality. Many photochemical and photothermal reactions in functional materials enable actuation such as in liquid crystal polymers,[16–23] in hydrogels and bilayered polymers filled with nanomaterials,[24–28] in shape-memory polymers,[29] as well as nickel-hydroxide-oxyhydroxide-based composites.[30] Due to specific constraints of the underlying reaction, these mate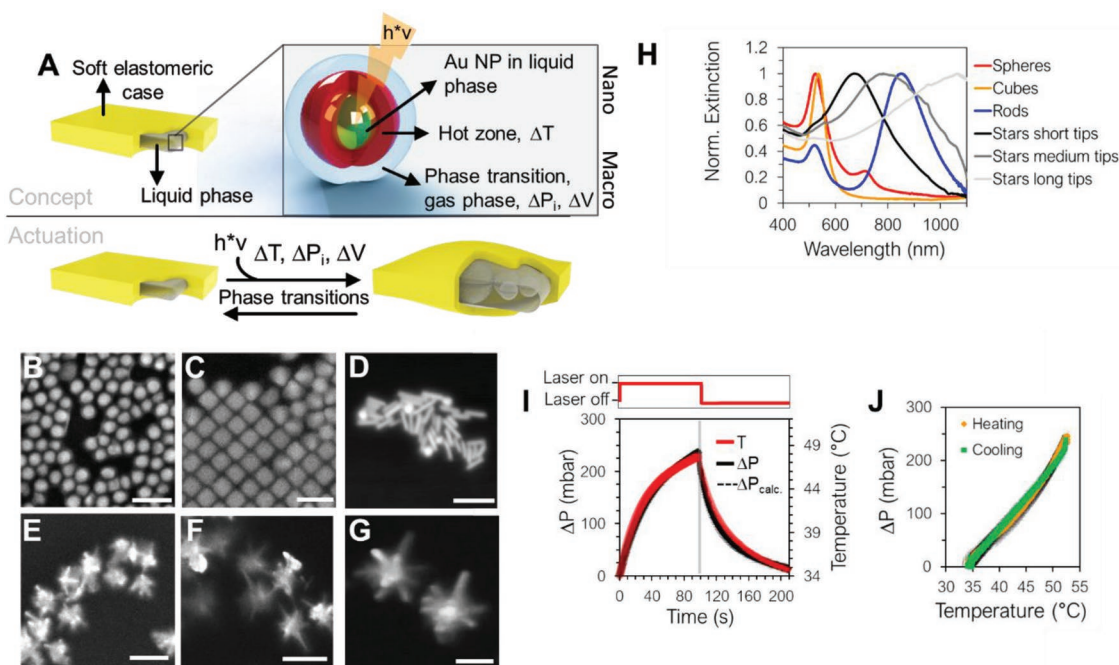rials may be restricted to certain environments or perform efficiently only at the microscale. Yet, light-driven fluidic actuation on the macroscale of an elastic soft structure has not been realized but could be highly beneficial for the emerging field of soft robotics.

Here, we create for the first time light-induced macroscale fluidic actuation that inflates an elastic structure due to a phase-transition driven by plasmonic heating of concentrated plasmonic nanoparticles (NPs) a liquid phase. The efficiency of plasmonic heating can easily be adapted tuning the plasmon resonance peak by altering NP's nanoscale shape (spherical, cubic, rod-like, star-like. etc.), its composition and size.[31,32] Plasmonic heating was already translated into actuation mechanisms.[33] Heat-induced shape changes of hydrogels actuate microswimmers[34,35] or control flow in a microchannel.[36] Melting and recrystallization or thermal expansion of polymers loaded with Au NPs induce reversible shape changes.[37,38] A nanotransduction was achieved by controlling van der Waals forces in polymer coatings on Au NPs by plasmonic heating.[39] Again, these actuators typically act in the microscale and typically only in water. To overcome these restrictions, we use the ability of the rapid liquid–gas phase transitions upon plasmonic heating[40,41] to create the pressure for fluidic actuation of an elastic structure. As the phase transition is encapsulated in the elastomer, it can be actuated in different environments (air, water, biological tissue) in the same configuration and it is

Figure 1. Concept, plasmonic structures, and light-induced pressure generation. A) Schematic of the concept and mechanism of light-driven inflation of a multiphase elastomeric actuator. A soft elastomer filled with a liquid phase containing metallic NPs converts light into heat at plasmon resonance. This induces a liquid-to-gas phase transition creating a volume increase, ΔV, and pressure, ΔP, inflating the elastic casing. Condensation-driven gas-to-liquid phase transition and pressure drop renders the actuation reversible. B–G) SEM images of nanostructured Au NPs: spherical, cubic, rod-shaped, star-shaped short spikes, star-shaped medium spikes, star-shaped long spikes NPs, respectively (scale bars 100 nm). H) Au NPs extinction spectra as function of wavelength and NP shape specifying plasmon resonance peaks, samples corresponding to NPs in (B)–(G). I) Pressure generation, ΔP, by plasmonic heating of rod-shaped Au NPs in methanol (80 µL, 3×10^{14} NPs L^{-1}) under continuous wave irradiation (808 nm, 475 mW cm^{-2}) in a closed, rigid container and pressure drop when laser is turned off. ΔP is perfectly described by the Antoine's equation ($\Delta P_{calc.}$, dashed line, overlaying with experimental data, average and standard deviation of six cycles). J) Pressure variation as function of temperature of dispersions of the rod-shaped Au NPs in methanol during heating and cooling cycles (average and standard deviation of six cycles).

efficient enough to drive various centimeter-scale soft robotic structures validating broad applicability.

Figure 1A shows the concept of the remotely light-powered actuation: laser irradiation heats metallic NPs at plasmon resonance dispersed in a liquid-phase that is encapsulated in an elastomeric casing. The liquid phase undergoes a phase transition and evaporates creating a pressure that inflates the elastomers. In an initial step, a library of Au NPs with distinct shapes was synthesized (Figure 1B–G) to achieve structures with different plasmon resonance peaks and to obtain nanoscale heating elements. None of the synthetic procedures requires complex laboratory equipment and all of them are based on well-established procedures detailed in the Supporting Information section. The Au NP structure-dependent plasmon resonance at which light absorption is highest (Figure 1H) result in most efficient heating when illuminated at peak wavelengths. Figure S1 (Supporting Information) shows concentration and structure-dependency of light-driven plasmonic heating of these particles (refs. [31,42] provide a theoretical background). Among the tested shapes, the rod- and medium-spiked star-shaped Au NPs expectedly showed most rapid heating at NIR frequency (808 nm) according to their resonance peaks close to excitation wavelength. Also other Au NPs shapes and other metallic nanostructures like silver-based NPs (Figure S2, Supporting Information) enable efficient heating when irradiated at resonance[42,43] and can be used to tailor absorption toward

specific wavelengths if other or multiple light sources are desired for driving heating. Generating complex structures (such in Figure S3, Supporting Information) can even tune NPs to respond to certain polarizations of light[44] which may give in future additional opportunities to control plasmon excitation patterns by the light source and NP shapes.

In a next step, the NPs were concentrated and dispersed in a phase changing medium with desired vapor pressure, e.g., water, ethanol, methanol. A postsynthetic surface functionalization of the Au NPs with poly(vinylpyrrolidone) was necessary to disperse the Au NPs in the liquids and to avoid aggregation-induced shifts in the plasmon resonances that may reduce performance of the actuators.

Most experiments have been performed using rod-shaped Au NPs with an average length of 43 ± 8 nm and width of 9 ± 1 nm (Figure 1D) dispersed in methanol (concentration $\approx 3 \times 10^{14}$ NPs L^{-1}). The as-synthesized rod-shaped Au NPs have a narrow plasmon peak in the NIR region at about 850 nm (full width at half maximum (FWHM) = 170 nm) at which efficient heating can be achieved (rod-shaped particles not only shift the plasmon peak but also increase heating efficiency by about 60% compared to spheres of the same volume[31]). Light-powered heating of methanol, ethanol, and water containing the rod-shaped Au NPs (evaporation kinetics given in Figure S4, Supporting Information) shows that the temperature variation, ΔT, is expectedly high enough to break up

ADVANCED
SCIENCE NEWS

www.advancedsciencenews.com

ADVANCED
MATERIALS

www.advmat.de

intermolecular attractive forces and to induce phase transitions and evaporation of the liquids. This eventually creates a pressure, ΔP, that depends on the thermodynamic properties of the liquid phase as well as the heat source. Methanol, as a potential phase transition medium, has a moderate boiling point of 64.7 °C at atmospheric pressure and its vapor pressure as function of temperature is given in Figure S4B (Supporting Information). Figure 1I shows the kinetics of temperature and pressure increase of 80 µL NPs dispersion containing 2×10^{10} rod-shaped Au NPs (a total of ≈1 µg gold) in methanol in a closed, inelastic container under irradiation by a continuous laser operating at 808 nm and a power of 475 mW cm^{-2}. In the first 30 s, heating and pressure increase almost linearly with rates of 0.43 °C s^{-1} and 4.3 mbar s^{-1}, respectively, then reducing to about 0.06 °C s^{-1} and 1.2 mbar s^{-1}, respectively. It is expected that the generated pressure variation, ΔP, is a result of the liquid-gas phase transition of methanol and hence the correspondingly created vapor pressures can be estimated by Antoine's equation, $\log_{10} P_{\mathrm{calc}} = A - \left(\frac{B}{C+T} \right)$, with A, B, and C being component-specific empiric constants obtained from database,[45] see Figure S5 (Supporting Information) for further details. Indeed, comparing measured ΔP with the predicted values shows exact description of the generated pressures by the model. When the laser is turned off, cooling initiates immediately with a rate constant of about 0.47 °C s^{-1} leading to a pressure decrease of about 5.9 mbar s^{-1} in the first 20 s, and logarithmically decreasing until reaching the initial temperature and pressure after about 120 s. The cooling process and depressurizing includes the reversible phase transition which is now condensation-driven and the cooling kinetics is again perfectly described by Antoine's equation at given temperatures. Figure 1J shows ΔP for the heating and cooling cycles, which correlate for both phase transitions with the temperature variation—either mainly determined by plasmonic heating under irradiation or by heat dissipation and condensation when the laser is turned off.

It follows that plasmonic-heating-induced phase transitions in an elastic container would result in inflation and elastic deformation. We thus merged two layers of silicone elastomers (Ecoflex 0030, 0.3–0.5 mm thick) separated by a floating spacer to form a 25 mm² flat pocket into which NP-solutions were added to achieve the actuator as depicted in Figure 1A. Movie S1 (Supporting Information) shows a video of the straightforward fabrication. To create preferential bulging in a certain direction, elastomers with variable degree of crosslinking and Young moduli were used for top and bottom layer, respectively (i.e., Ecoflex 0030 for top layer and Dragon Skin 20) or the bottom layer was chosen at least ten times thicker than the top layer. Before injecting the NPs solution into the pocket, the pressure-extension relationship of the elastomeric pocket was tested by pressurizing it with methanol and a syringe pump. The setup is schematized in **Figure 2**A in which, during pressurizing, the elevation of a cantilever (32 mm length, 3 mg) attached to one side of the elastomeric pocket was observed. The results are given in Figure 2B showing that at a given maximal ΔP of ≈240 mbar (maximal ΔP obtained with AuNPs in the closed container) a displacement, Δh, of the cantilever of up to 11 mm and variation of the angle, $\Delta \alpha$, of ≈25° can be projected. The deformation of an inflated elastomeric membrane depends on the pressure,

on the geometry of the membrane and its constraint, as well as the stress-strain relation of its material.[46–48] Numerical simulations (Figure S6, Supporting Information) confirm that cantilever displacement reflects the deformation of the elastic membrane at different pressures and given dimensions and materials. The four edges of the membrane are considered fully constrained, as in the actuator. The measured data for Δh and $\Delta \alpha$ in the given pressure interval, however, can be estimated with an acceptable accuracy for our elastic pocket by the exponential equation $\Delta h = 20(1 - e^{-0.0044\Delta P})$, $R^2 = 0.96$ thus providing an approximation of the internal pressure by measuring Δh. We then injected rod-shaped Au NPs dispersed in methanol (20 µL, 3×10^{14} NPs L^{-1}) into the same pocket followed by on–off laser irradiation to initiate phase transitions. Figure 2C and D shows kinetics of ΔT, Δh, and $\Delta \alpha$ profiles under laser irradiation, respectively. Movie S2 (Supporting Information) shows a multicycle actuation. As expected from results given in Figure 1, the temperature of the NP solutions rises by about 20°C during continuous laser exposure for 180 s reaching a maximum of 52 °C after ≈150 s. In a similar manner, due to the phase transition induced inflation, the cantilever is actuated resulting in Δh and $\Delta \alpha$ reaching a maximal variation of 2.2 mm and 5.2° under the experimental conditions. The kinetics shows that heating and displacement are strongly dependent on—and thus controllable by—laser irradiation time and the laser intensity (Figure S7 in the Supporting Information gives cantilever displacement as function of laser intensity). Translucency of the elastic materials as function of thickness and wavelength of light is given in Figure S8 (Supporting Information). As the plasmon excitation occurs through the elastomers, light absorption of the elastic material itself should be as low as possible to decrease loss of intensity and heating of the membrane. This can be done by tailoring elastomers, laser wavelength and power and nanoparticle's plasmon peak. The absorption of the elastomers used here did not affect actuation and no cantilever displacement was observed when the actuator is irradiated when filled only with the phase changing medium without Au NPs (Figure S9, Supporting Information). When the laser is turned off, temperature drops correspondingly and h decreases first rapidly (in the first 30 s by ≈50% with a rate of 32 µm s^{-1}), then continuously approaching initial conditions similar as in the measurements in the inelastic, closed container. Figure 2E shows the pressure variation $\Delta P_{\mathrm{calib.}}$ in the elastic pocket estimated using Δh and the calibration of the displacement given in Figure 2B. Maximum displacement occurred along with an internal pressure increase of ≈26 mbar. During laser-off period, the temperature and pressure decreases, and the displacement and corresponding pressure variations are reversible to about ≈65% within 200 s. Figure S10 (Supporting Information) shows that further reducing the external temperature from about 25 to 4 °C for 20 min or increasing relaxation periods to 60 min, did not lead to a 100% reversibility of Δh as previously obtained for ΔP in the closed vessel (Figure 1J). Eliminating the time constant by plotting the temperature-pressure relationship (Figure 2F) indicates—although again largely reversible—a lag of ΔP between heating and cooling cycles. This can be an effect of the heat transfer properties of silicone elastomers that may decelerate condensation (thermal conductivity of Ecoflex 0030 is ≈0.16 W m^{-1} K^{-1} and the parameter typically decreases
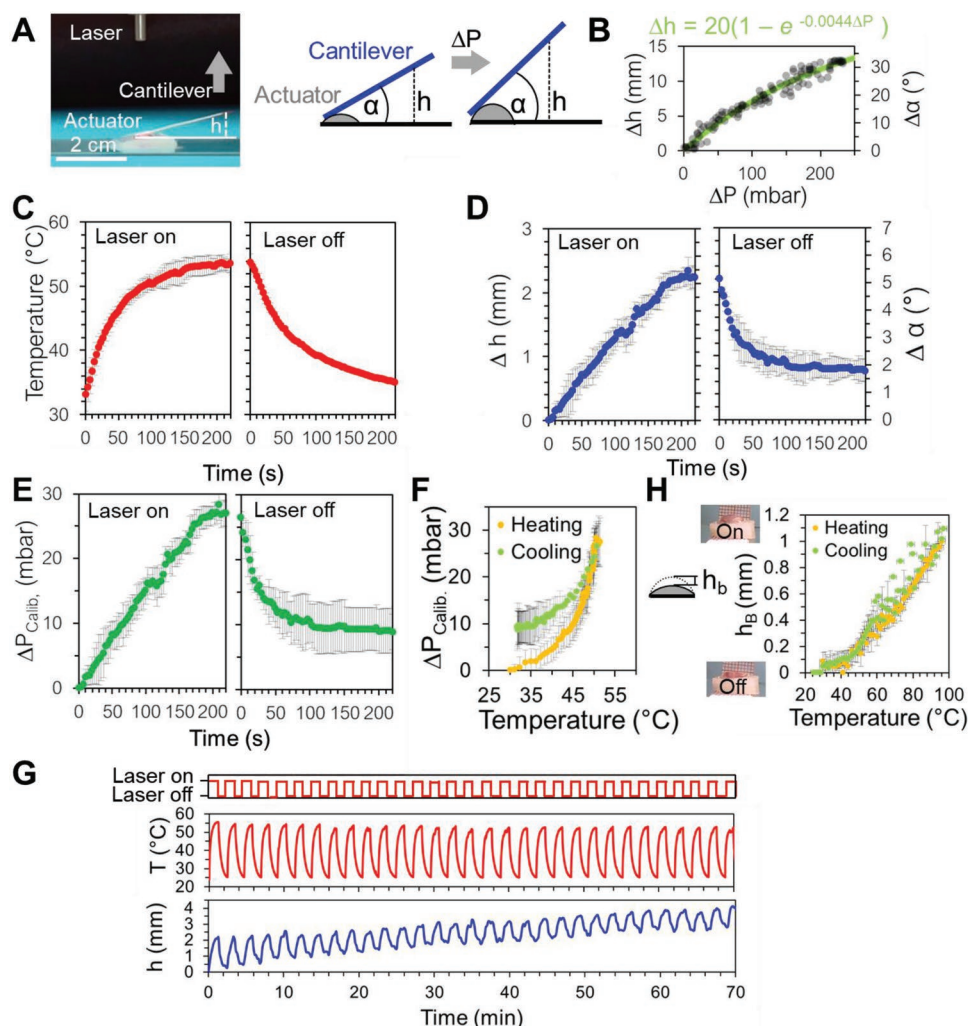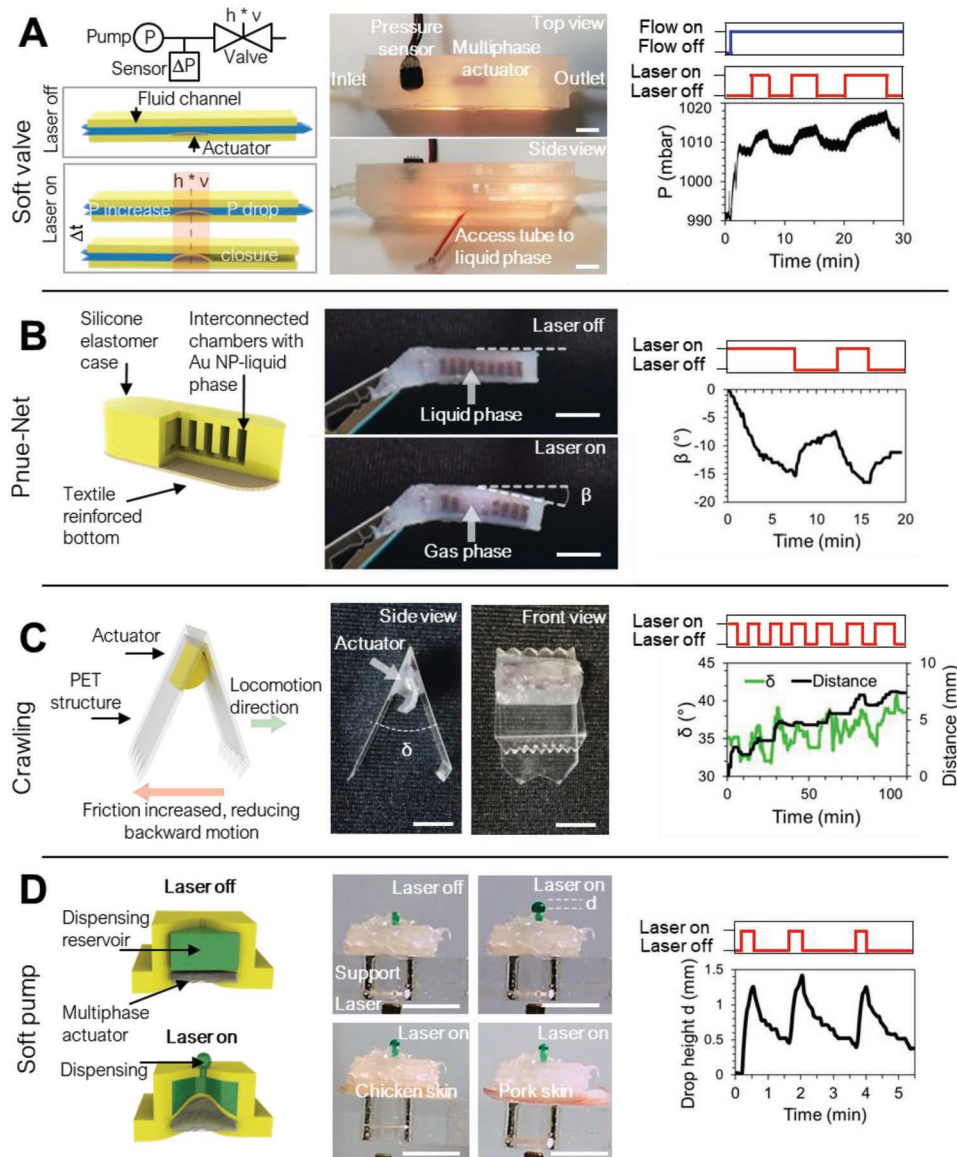
Figure 2. Remotely powered, light-driven inflation, and actuation of elastomers. A) Image and schematic of the characterization arrangement for elastomeric multiphase actuators. A cantilever is attached at the side of the inflating pocket. Actuation and elastic deformation is documented in terms of vertical displacement of the cantilever, Δh. B) Characterization of elastic deformation and the internal pressure variation during controlled injection of methanol by a motor-driven syringe pump and simultaneous pressure sensing. C,D) Temperature variation, cantilever displacement, and pressure ($\Delta P_{calib.}$ calculated from Δh using correlation in (B), respectively, during laser irradiation (808 nm, 475 mW cm^{-2}) and laser-off periods when silicone-based actuator is filled with rod-shaped Au NPs (20 µL, 3×10^{14} NPs L^{-1}); average and standard deviations of five measurements. F) Pressure variation as function of temperature for actuator described in (C) and (D). H) Temperature–displacement relationship for heating and cooling cycles of an SEBS-based elastomeric phase-transition actuator during laser on–off cycles (20 µL Au NPs in methanol, 3×10^{14} NPs L^{-1}) plotted in terms of the displacement of the bulging surface, h_b (average and standard deviation of three measurements), see also Movie S3 (Supporting Information). G) Temperature and cantilever displacement during a multicycle stimulation of a silicone-based actuator filled with rod-shaped Au NPs in methanol (20 µL, 3×10^{14} NPs L^{-1}, laser irradiation at 808 nm, 475 mW cm^{-2}) with an average displacement of 1.4 ± 0.3 mm per cycle.

with elastic modulus of the material.[49] A further aspect is the partial permeability of silicone elastomers for gasses such as methanol which permits a certain level of continuous loss of liquid phase through the silicone casing influencing internal pressure. To investigate this aspect, we measured methanol permeation through silicone elastomers, a paraffin-modified silicone, and a styrene–ethylene–butylene–styrene (SEBS)-based elastomer reported in Figure S11 (Supporting Information). Paraffin-modification of silicone slightly reduced gas permeability as reported previously,[50] however, truly marginal gas penetration was only observed by changing the elastic material to the SEBS-based elastomer. Indeed, producing a similar actuator made of SEBS rendered expansion of the elastomers

during heating and cooling cycles reversible given by the temperature-actuation relationship in Figure 2G. Movie S3 (Supporting Information) shows the SEBS-based actuator and lifting a weight of ≈200 times the weight of the liquid phase during laser on–off cycles. The energy conversion efficiency is thereby several magnitudes higher than light-driven actuators operating at the microscale[51] and a magnitude higher as a recent example of a soft light-driven macroscale actuator (Figure S12a for further details, Supporting Information). Nevertheless, also with silicone elastomers, the displacement is largely repeatable and Figure 2H shows a 30-cycle on–off stimulation, corresponding temperature and displacement of the actuator. The results confirm that heating and displacement are

replicable at the given time intervals (1 min on, 1 min off) and a persistent Δh of 1.4 ± 0.3 mm per cycle (average ΔT per cycle 30 °C) is achieved, independent of the h at which the cycle started. The absolute displacement thereby correlates with ΔT, which is itself highly repeatable. The achieved performance

in terms of maximal pressure through the plasmonic phase transition ($\Delta p = 230$ mbar in rigid container, 26 mbar in soft actuator, Figures 1 and 2) observed in our experiments is in a similar magnitude of a recently published tethered soft pump based on electrohydrodynamic mechanism achieving 140 mbar[52]

Figure 3. Integration of light-driven inflating elastomers as remotely powered actuators in soft robotic scenarios. A) Realization of a light-driven soft valve. Left panel: schematic of the concept and fluidic circuit of a channel (5 mm width, 1 mm height) with integrated light-driven multiphase actuator. Upon laser irradiation, phase-transition causes bulging of the elastic layer and continuously closes the channel. Middle panel: photographs of silicon-based channel with multiphase actuator. Right panel: the pressure variation measured between inlet and valve during laser on–off cycling. B) Light-powered directional bending of silicone-based pneu-net structure filled with Au NP-loaded methanol phase. Upon laser irradiation, liquid–gas phase transition occurs and leads to bending by angle β (middle panel and right panel, respectively). This is largely reversible during laser-off cycles and the structure moves back. C) Light-driven crawling structure actuated by an integrated multiphase actuator. Upon laser on–off cycles, the actuator expands and contracts opening and closing of the crawling structure and forward movement (schematized and imaged in first and second panels, respectively). Right panel: angle δ and crawling distance during seven laser on–off cycles. D) Realization of a light-driven soft pump. Left panel: schematic of the soft pump with two isolated silicone chambers: the lower chamber contains the Au-NPs-loaded liquid phase and is separated by a silicone layer from the upper dispensing chamber with the outlet. Upon laser irradiation, inflation pumps the liquid out of the dispensing chamber. Due to the NIR penetration in biological tissue, the pump can be actuated through peeled chicken and porcine skin (middle panel, see Movie S8 in the Supporting Information for biological samples of different thickness). Right panel: dispensing in terms of drop height controlled by laser irradiation and on–off cycles. In all experiments methanol containing rod-shaped Au NPs (3×10^{14} NPs L^{-1}) were used as liquid phase and irradiated with 808 nm laser at 475 mW cm^{-2}. Scale bars are 1 cm.

(see Figure S12b in the Supporting for a comparison of the maximal pressures of this and soft/flexible material-based pumps based on other principles[52–57]). We believe that further adapting and tailoring actuator shapes elastic and plasmonic materials and excitation is a manner to yet elevate these metrics.

Nevertheless, essential aim of this work is to develop a light-powered actuation system which can easily be integrated with other components and moreover operate in different environments. **Figure 3** confirms the compatibility of the light-powered multiphase materials as actuators in various applications, in a soft valve, a pnue-net bending structure, a crawling robot, and a pump, Figure 3A–D. Figure 3 left and middle panels present concept and images, respectively of a soft valve, which can be controlled by external laser irradiation. The light passes through the semitransparent silicon-based material in which the actuator is integrated in a channel (5 mm width, 1 mm height). Upon laser irradiation, the bulging layer of the actuators, which has a lower modulus (100% modulus = 10 psi, Ecoflex 0030,[58]) compared to the channel (22 psi, Dragon Skin 20,[58]), preferentially inflates and continuously closes the channel. This can be determined by measuring the pressure increase between the inlet pump and the valve during continuous liquid flow. The absolute pressure during three on–off cycles is given in Figure 3A, right panel. Movie S4 (Supporting Information) shows light-driven actuation and complete closure of the channel as depicted in the schematics in Figure 3, left panel.

Furthermore, a pnue-net structure,[59] obtained by casting a 3D printed mold, enables a bending motion that can be actuated by light after incorporating the Au-NPs-containing liquid into the interconnected chambers of the inner structure, Figure 3B, left panel. Remote laser irradiation causes controllable bending due to the phase transitions in the interconnecting chambers depicted in Figure 3B, middle and right panels. The bending angle, β, can thereby be controlled by laser irradiation intervals (Figure 3B, right panel, and Movie S5, Supporting Information).

The integrability of the soft actuators with other components is further presented in terms of actuation of a crawling structure consisting of a centimeter scale poly(ethylene terephthalate) sheet. The structure enables directional forward locomotion while reducing backward motion by selectively increasing friction with the substrate using oriented hooks as shown in Figure 3C, left and middle panels. The multiphase actuator is placed between the two sides and laser on–off cycling causes the actuator to reversibly expand and contract resulting in opening and closing of the structure described by angle δ. Forward locomotion of ≈1 mm per laser on–off cycle is observed as shown Figure 3C, right panel and Movie S6 (Supporting Information). The centimeter-scale crawling structure has a weight of ≈1 g including an Au-NPs-containing liquid phase of 80 µL driving locomotion which corresponds to only ≈6% its total weight.

Perhaps one of the most interesting applications could arise from a realization of a soft pumping/dispensing system such as shown in Figure 3D (overview soft assembly components in Figure S13, Supporting Information). Thereby the remotely light-powered multi-material actuator (with 20 µL Au NPs in methanol, 3×10^{14} NPs L^{-1}) is incorporated in a silicon-based assembly which contains an isolated reservoir filled with a dispensing liquid. Remote laser irradiation leads to inflation of the actuation chamber. This decreases the volume of the reservoir and causes dispensing. The concept of the pump is shown in Figure 3D, left panel and Movie S7 (Supporting Information) shows its operation. The liquid phase causing actuation is notably only 1.5% of total pump weight. Figure 3D panel 2 shows images of the experiments in which the pump is activated by laser on–off cycling as well as through peeled skin samples (chicken and porcine skin containing also dermis and connective tissue, see Figure S14 (Supporting Information) for biological sample description). Due to the NIR light penetration in biological tissue the pump is performing and such a system may have perspectives as, e.g., a drug delivery system which can be controlled and powered externally through the biological tissue. Movies S7 and S8 (Supporting Information) show the pumping by droplet formation and as function of type and thickness of the biological tissue. Panel three of Figure 3D shows the kinetics of a drop continuously and rapidly forming under laser irradiation (475 mW cm^{-2}). After about 20 s a drop height of 1 mm, corresponding to a dispensed volume of 4 µL (considering the drop as a half sphere) is achieved before laser is turned off to begin a new cycle. The dispensing volume can be precisely controlled by irradiation time and laser intensity. An advantage is that the actuating phase transition is spatially isolated from the dispensing liquid and the surrounding environment. The system is indeed suited to be used in the same configuration in different environments and we show this by remotely-powering the same pump immersed under water and being fully functional for dispensing (Movie S9, Supporting Information). In conclusion of the experiments presented in Figure 3, the following key application scenarios can be projected. Valves and precisely controllable pumps are key components in microfluidics and the light-driven soft actuators can be combined into integrated untethered microfluidic devices in which an external laser operates and remotely powers the device. The general capability to drive fluidic actuation and forward-motion and bending, respectively is essential for soft robotics and soft micromanipulation in cases in which light-driven powering is advantageous. This can be particularly interesting for biomedical purposes and untethered in vivo soft devices that can be controlled from outside the tissue in a manner that is less invasive as tethered systems. The results confirm that the actuator can be operated through barriers like biological tissue.

Experimental Section

Supporting Information

Supporting Information is available from the Wiley Online Library or from the author.

[1] V. Kumar, M. Taddeo, P. E. Dupont, G.-Z. Yang, R. Wood, Z. L. Wang, P. Fischer, M. Veloso, N. Jacobstein, R. Merrifield, B. J. Nelson, B. Scassellati, J. Bellingham, M. McNutt, R. Full, L. Floridi, R. Taylor, *Sci. Rob.* **2018**, *3*, eaar7650.

[2] S. I. Rich, R. J. Wood, C. Majidi, *Nat. Electron.* **2018**, *1*, 102.

[3] G. M. Whitesides, *Angew. Chem., Int. Ed.* **2018**, *57*, 4258.

[4] D. Rus, M. T. Tolley, *Nature* **2015**, *521*, 467.

[5] P. Polygerinos, N. Correll, S. A. Morin, B. Mosadegh, C. D. Onal, K. Petersen, M. Cianchetti, M. T. Tolley, R. F. Shepherd, *Adv. Eng. Mater.* **2017**, *19*, 1700016.

[6] B. Gorissen, D. Reynaerts, S. Konishi, K. Yoshida, J. W. Kim, M. De Volder, *Adv. Mater.* **2017**, *29*, 1604977.

[7] Y. Forterre, *J. Exp. Bot.* **2013**, *64*, 4745.

[8] S. Li, K. W. Wang, *Bioinspiration Biomimetics* **2017**, *12*, 011001.

[9] M. Wehner, M. T. Tolley, Y. Mengüç, Y.-L. Park, A. Mozeika, Y. Ding, C. Onal, R. F. Shepherd, G. M. Whitesides, R. J. Wood, *Soft Rob.* **2014**, *1*, 263.

[10] B. F. Haynes, W. Chen, Y. Feng, D. S. Dimitrov, G. Kelsoe, S. C. Harrison, T. B. Kepler, N. S. Longo, D. E. Russ, H. W. Sun, P. E. Lipsky, S. Kupriyanov, *Science* **2015**, *349*, 161.

[11] A. Miriyev, K. Stack, H. Lipson, *Nat. Commun.* **2017**, *8*, 596.

[12] M. Wehner, R. L. Truby, D. J. Fitzgerald, B. Mosadegh, G. M. Whitesides, J. A. Lewis, R. J. Wood, *Nature* **2016**, *536*, 451.

[13] R. F. Shepherd, A. A. Stokes, J. Freake, J. Barber, P. W. Snyder, A. D. Mazzeo, L. Cademartiri, S. A. Morin, G. M. Whitesides, *Angew. Chem., Int. Ed.* **2013**, *52*, 2892.

[14] M. T. Tolley, R. F. Shepherd, B. Mosadegh, K. C. Galloway, M. Wehner, M. Karpelson, R. J. Wood, G. M. Whitesides, *Soft Rob.* **2014**, *1*, 213.

[15] A. D. Marchese, C. D. Onal, D. Rus, *Soft Rob.* **2014**, *1*, 75.

[16] T. Ikeda, J. I. Mamiya, Y. Yu, *Angew. Chem., Int. Ed.* **2007**, *46*, 506.

[17] M. Yamada, M. Kondo, J. I. Mamiya, Y. Yu, M. Kinoshita, C. J. Barrett, T. Ikeda, *Angew. Chem., Int. Ed.* **2008**, *47*, 4986.

[18] H. Jiang, C. Li, X. Huang, *Nanoscale* **2013**, *5*, 5225.

[19] L. Hines, K. Petersen, G. Z. Lum, M. Sitti, *Adv. Mater.* **2017**, *29*, 1603483.

[20] S. Palagi, A. G. Mark, S. Y. Reigh, K. Melde, T. Qiu, H. Zeng, C. Parmeggiani, D. Martella, A. Sanchez-Castillo, N. Kapernaum, F. Giesselmann, D. S. Wiersma, E. Lauga, P. Fischer, *Nat. Mater.* **2016**, *15*, 647.

[21] H. Zeng, C. Xuan, D. S. Wiersma, P. Wasylczyk, *Adv. Opt. Mater.* **2016**, *4*, 1689.

[22] H. Zeng, O. M. Wani, P. Wasylczyk, R. Kaczmarek, A. Priimagi, *Adv. Mater.* **2017**, *29*, 1701814.

[23] O. M. Wani, H. Zeng, A. Priimagi, *Nat. Commun.* **2017**, *8*, 15546.

[24] H. Koerner, G. Price, N. A. Pearce, M. Alexander, R. A. Vaia, *Nat. Mater.* **2004**, *3*, 115.

[25] E. Wang, M. S. Desai, S. W. Lee, *Nano Lett.* **2013**, *13*, 2826.

[26] X. Zhang, Z. Yu, C. Wang, D. Zarrouk, J. W. T. Seo, J. C. Cheng, A. D. Buchan, K. Takei, Y. Zhao, J. W. Ager, J. Zhang, M. Hettick, M. C. Hersam, A. P. Pisano, R. S. Fearing, A. Javey, *Nat. Commun.* **2014**, *5*, 2983.

[27] L. Chen, M. Weng, P. Zhou, L. Zhang, Z. Huang, W. Zhang, *Nanoscale* **2017**, *9*, 9825.

[28] B. Han, Y.-L. Zhang, Q.-D. Chen, H.-B. Sun, *Adv. Funct. Mater.* **2018**, *28*, 1802235.

[29] M. Behl, A. Lendlein, *Mater. Today* **2007**, *10*, 20.

[30] K. W. Kwan, S. J. Li, N. Y. Hau, W. Li, S. P. Feng, A. H. W. Ngan, *Sci. Rob.* **2018**, *3*, eaat4051.

[31] G. Baffou, R. Quidant, C. Girard, *Appl. Phys. Lett.* **2009**, *94*, 153109.

[32] Z. Wu, S. Yang, W. Wu, *Nanoscale* **2016**, *8*, 1237.

[33] Y. Hu, Z. Li, T. Lan, W. Chen, *Adv. Mater.* **2016**, *28*, 10548.

[34] A. Mourran, H. Zhang, R. Vinokur, M. Möller, *Adv. Mater.* **2017**, *29*, 1604825.

[35] H. Zhang, A. Mourran, M. Möller, *Nano Lett.* **2017**, *17*, 2010.

[36] S. R. Sershen, G. A. Mensing, M. Ng, N. J. Halas, D. J. Beebe, J. L. West, *Adv. Mater.* **2005**, *17*, 1366.

[37] F. Ge, X. Lu, J. Xiang, X. Tong, Y. Zhao, *Angew. Chem., Int. Ed.* **2017**, *56*, 6126.

[38] B. Han, Y. Y.-L. Zhang, L. Zhu, Y. Li, Z.-C. Z. Ma, Y.-Q. Y. Liu, X. X.-L. Zhang, X.-W. X. Cao, Q.-D. Q. Chen, C. C.-W. Qiu, H.-B. H. Sun, *Adv. Mater.* **2018**, *31*, 1806386.

[39] T. Ding, V. K. Valev, A. R. Salmon, C. J. Forman, S. K. Smoukov, O. A. Scherman, D. Frenkel, J. J. Baumberg, *Proc. Natl. Acad. Sci. USA* **2016**, *113*, 5503.

[40] Y. Wang, M. E. Zaytsev, H. Le The, J. C. T. Eijkel, *ACS Nano* **2017**, *11*, 2045.

[41] G. Baffou, J. Polleux, S. Monneret, *J. Phys. Chem. C* **2014**, *118*, 4890.

[42] A. O. Govorov, H. H. Richardson, *Nano Today* **2007**, *2*, 30.

[43] Y. Wang, P. H. C. Camargo, S. E. Skrabalak, H. Gu, Y. Xia, *Langmuir* **2008**, *24*, 12042.

[44] N. H. Cho, W. S. Kim, M. Kim, J. Rho, Y. Y. Lee, K. Chang, H.-Y. Ahn, K. T. Nam, J. Mun, H.-E. Lee, *Nature* **2018**, *556*, 360.

[45] Dortmund Data Bank, www.ddbst.com (accessed: April 2019).

[46] W. W. Feng, P. Huang, *J. Appl. Mech.* **1974**, *41*, 767.

[47] W. H. Yang, W. W. Feng, *J. Appl. Mech.* **1970**, *37*, 1002.

[48] D. Steck, J. Qu, S. B. Kordmahale, D. Tscharnuter, A. Muliana, J. Kameoka, *J. Appl. Polym. Sci.* **2019**, *136*, 47025.

[49] M. D. Bartlett, N. Kazem, M. J. Powell-palm, X. Huang, W. Sun, J. A. Malen, C. Majidi, *Proc. Natl. Acad. Sci. USA* **2017**, *114*, 2143.

[50] K. Ren, Y. Zhao, J. Su, D. Ryan, H. Wu, *Anal. Chem.* **2010**, *82*, 5965.

[51] H. Okamura, K. Yamaguchi, R. Ono, *Int. J. Optomechatronics* **2009**, *3*, 277.

[52] V. Cacucciolo, J. Shintake, Y. Kuwajima, S. Maeda, D. Floreano, H. Shea, *Nature* **2019**, *572*, 516.

[53] O. Chan, S. Wook, S. Sik, J. Jungho, *Sens. Actuators, A* **2005**, *124*, 453.

[54] A. Jahanshahi, F. Axisa, J. Vanfleteren, *Proc. SPIE* **2011**, *7929*, 79290R.

[55] C. Stergiopulos, D. Vogt, M. Tolley, M. A. Wehner, in *Proc. ASME 2014 Conference on Smart Materials, Adaptive Structures and Intelligent Systems SMASIS2014*, **2014**, https://doi.org/10.1115/SMASIS2014-7536.

[56] B. C. Mac Murray, X. An, S. S. Robinson, I. M. Van Meerbeek, K. W. O. Brien, H. Zhao, R. F. Shepherd, *Adv. Mater.* **2015**, *27*, 6334.

[57] M. Loepfe, C. M. Schumacher, W. J. Stark, *Ind. Eng. Chem. Res.* **2014**, *53*, 12519.

[58] S.-O. Inc., Technical Data Provided by the Supplier's Technical Bulletin, **2018**.

[59] B. Mosadegh, P. Polygerinos, C. Keplinger, S. Wennstedt, R. F. Shepherd, U. Gupta, J. Shim, K. Bertoldi, C. J. Walsh, G. M. Whitesides, *Adv. Funct. Mater.* **2014**, *24*, 2163.

[60] M. R. K. Ali, B. Snyder, M. A. El-Sayed, *Langmuir* **2012**, *28*, 9807.

[61] H. Wang, Y. Liu, M. Li, H. Huang, H. M. Xu, R. J. Hong, H. Shen, *J. Mater. Chem. C* **2013**, *1*, 6861.

[62] P. Pallavicini, A. Donà, A. Casu, G. Chirico, M. Collini, G. Dacarro, A. Falqui, C. Milanese, L. Sironi, A. Taglietti, *Chem. Commun.* **2013**, *49*, 6265.

[63] R. D. Near, S. C. Hayden, R. E. Hunter, D. Thackston, M. A. El-Sayed, *J. Phys. Chem. C* **2013**, *117*, 23950.

1905671 (8 of 8)